Confined dynamics in spherical polymer brushes

Shivraj B. Kotkar,[†] Michael P. Howard,[‡] Arash Nikoubashman,[¶,§] Jacinta C. Conrad,[*,†] Ryan Poling-Skutvik,[*,‖] and Jeremy C. Palmer[*,†]

†*Department of Chemical and Biomolecular Engineering, University of Houston, Houston, TX 77204*

‡*Department of Chemical Engineering, Auburn University, Auburn, AL 36849*

¶*Leibniz-Institut für Polymerforschung Dresden e.V., Hohe Straße 6, 01069 Dresden, Germany*

§*Institut für Theoretische Physik, Technische Universität Dresden, 01069 Dresden, Germany*

‖*Department of Chemical Engineering, University of Rhode Island, Kingston, RI 02881*

Received October 24, 2023; E-mail: jcconrad@uh.edu; ryanps@uri.edu; jcpalmer@uh.edu

Abstract: We investigate the dynamics of polymers grafted to spherical nanoparticles in solution using hybrid molecular dynamics simulations with a coarse-grained solvent modeled via the multi-particle collision dynamics algorithm. The mean-square displacements of monomers near the surface of the nanoparticle exhibit a plateau on intermediate time scales, indicating confined dynamics reminiscent of those reported in neutron spin-echo experiments. The confined dynamics vanish beyond a specific radial distance from the nanoparticle surface that depends on the polymer grafting density. We show that this *dynamical* confinement transition follows theoretical predictions for the critical distance associated with the *structural* transition from confined to semidilute brush regimes. These findings suggest the existence of a hitherto unreported dynamic length scale connected with theoretically predicted static fluctuations in spherical polymer brushes and provide new insights into recent experimental observations.

Grafting polymers to the surface of nanoparticles (NPs) can dramatically enhance dispersion in polymer nanocomposites,[1–5] reduce frictional interactions,[6,7] and improve the biocompatibility and delivery of drugs[8–11] and theranostics.[12–14] Beyond chemically modifying the surface, contributions from the extended structure and dynamic fluctuations of the grafted polymers can enhance their utility.[15–17] The structure and dynamics of grafted polymers are significantly perturbed from those of free chains for two reasons: the surface tether prevents fluctuations of the grafted end, and the surface localization of the chains increases the local monomer concentration.[18] For planar substrates and sufficiently high grafting density σ, these perturbations lead to extended chain conformations,[19–23] slower relaxations,[24,25] and the emergence of collective dynamics.[26–31]

When polymers are grafted to spherical (or cylindrical) NPs, however, the surface curvature set by the NP radius R_{NP} introduces a radial dependence to the monomer concentration and subsequently to the polymer conformations.[32–35] Scaling theories predict that the structure of brushes grafted to spherical NPs in a good solvent depends on σ and the radial distance r. At moderate σ, pairwise interactions between monomers lead to a semidilute polymer brush (SDPB) regime in which the brush height h scales with the number of repeat units N as $h \sim \left(N\sigma^{1/3}\right)^{3/5}$.[32,36] At larger σ, higher order segmental interactions dominate, leading to a more extended concentrated polymer brush (CPB) regime where $h \sim \left(N\sigma^{1/2}\right)^{\nu}$ with excluded volume parameter $3/5 \leq \nu \leq 1$. Because the local monomer concentration decreases with increasing r, brushes whose length exceeds a critical radius R_{CPB} transition continuously from the CPB regime near the NP surface to the SDPB regime at the periphery.[34] These grafted polymer conformations have been confirmed by simulations and experiments.[37–40]

Similar to structural perturbations, the dynamics of grafted chains deviate from those of free chains. Scaling theory predicts that the relaxation time of brushes scales as $\tau \sim N^3$,[41,42] slower than for free chains experiencing non-hydrodynamic Rouse ($\tau \sim N^2$) or hydrodynamically coupled Zimm ($\tau \sim N^{3\nu}$) relaxations.[18] The relaxation time of monomers varies non-monotonically with monomer position, with monomers near the chain center exhibiting the slowest relaxations.[39,43] Additionally, the intrachain relaxations of grafted polymers do not follow simple exponential decays.[39,44,45] Instead, neutron spin-echo (NSE) measurements find that grafted chains are confined by their neighbors and do not fully relax on observable time scales.[44,45] By selectively contrast matching the grafted chains, NSE measurements reveal that dynamics are slower in the CPB region than in the SDPB region of a long brush.[46] This behavior was confirmed in recent molecular dynamics (MD) simulations, which also showed that the relaxation time of individual chains increases with increasing confinement (i.e., increasing σ).[47,48] Although these investigations suggest that the relaxations of grafted polymers are affected by the local brush structure, a direct connection between brush structure and dynamics has not yet been demonstrated.

Here, we use hybrid MD simulations with a mesoscale solvent model to show that the confined dynamics of polymers grafted to spherical NPs originate from the strong crowding and extended conformation of chains in the CPB regime. In agreement with earlier studies,[39,43] the relaxation times extracted from the mean-squared displacements (MSDs) are maximal for monomers near the center of the chain, and increase with grafting density. For monomers near the particle surface, the MSDs exhibit plateaus on intermediate time scales. This intermediate-time plateau is consistent with the confined dynamics observed in NSE experiments,[44,45] but it has not been scrutinized in previous computational studies of spherical brushes.[39,48] The plateau value increases with increasing monomer position and finally disappears for monomers sufficiently far from the particle surface, suggesting a continuous transition from confined to unconfined dynamics. To characterize this transition, we determine the monomer position at which the dynamical confinement disappears and show that this position is comparable to R_{CPB}, which controls the structural transition between CPB and

SDPB regimes. Our findings therefore establish the structural origins underlying the confined, slow relaxations of grafted polymers.

We performed simulations of Kremer–Grest[49] bead–spring polymers end-grafted to a spherical NP. We included solvent-mediated hydrodynamic interactions (HI) by using an explicit, mesoscale solvent modeled using the multiparticle collision dynamics (MPCD) algorithm.[50–55] For convenience, we define a, m, ε, and $\tilde{t} = \sqrt{ma^2/\varepsilon}$ as the fundamental units for length, mass, energy, and time, respectively, and report model parameters and physical quantities from the simulations in dimensionless form based on these units. In what follows, these units are omitted for brevity. Each polymer chain consisted of 120 monomers with diameter $a_{\mathrm{P}} = 1$. The NP was modeled as a collection of monomer-sized beads positioned at 642 vertices on the surface of a sphere of radius $R_{\mathrm{NP}} = 5$, yielding a surface density of ≈ 2. The positions of the vertices were generated by recursively subdividing the faces of a regular icosahedron into equilateral triangles and then radially scaling the vertices to a distance R_{NP} from the center of the sphere.[56,57] Spring-like bonds between adjacent monomers on the polymer chains and between the end monomers and grafting sites on the NP surface were modeled using the finite extensible nonlinear elastic (FENE) potential.[58] Excluded volume interactions between monomer-monomer and monomer-NP beads were implemented using a purely repulsive Weeks-Chandler-Andersen (WCA) potential to mimic good solvent conditions.[59] A standard MPCD solvent with number density $\rho_{\mathrm{s}} = 5$ was used in conjunction with a momentum-conserving version of the Andersen thermostat,[60,61] resulting in a fluid with Schmidt number $\mathrm{Sc} \approx 12.0$ and dynamic viscosity $\eta_{\mathrm{s}} \approx 4.0$. The MPCD solvent was coupled to the polymer monomers and NP beads using the scheme in Ref. 62. Three reduced grafting densities were considered in the hybrid MD–MPCD simulations, $\gamma = \sigma R_{\mathrm{g},0}^2 = \{10, 25, 50\}$, where $R_{\mathrm{g},0} = 8.3$ is the radius of gyration of a free 120-mer chain in an infinitely dilute solution. These values were chosen to fall within the range probed in recent experiments.[45] Additional grafting densities ranging from $\gamma = 0.22$ to 50 were considered in a complementary set of implicit-solvent Langevin dynamics (LD) simulations to investigate brush dynamics in the absence of HI. All simulations were performed at a reduced temperature $T = 1$. Additional details of the models and simulation protocols are presented in Supporting Information. Chain dynamics were characterized *via* the time-dependent mean-squared displacements $g_i(t) = \langle[\mathbf{r}_i(t) - \mathbf{r}_i(0)]^2\rangle$ of individual monomers, where i is the monomer index (1 for the grafted monomer and 120 for the free end); the angle brackets $\langle\cdots\rangle$ denote that the average is taken over multiple time origins with the same lag time t for monomers with the same index on different chains. The monomer position vector $\mathbf{r}_i = (x_i, y_i, z_i)$ is defined relative to the reference frame of the NP center of mass. The total MSD was also decomposed in the directions perpendicular and parallel to the NP surface to characterize anisotropy of the chain dynamics; the perpendicular and parallel components $g_{i,\perp}$ and $g_{i,\parallel}$ were defined to be colinear and orthogonal to the vector $\mathbf{r}_i(0)$, respectively (Supporting Information, Fig. S1).

The resulting MSDs follow the expected behavior for grafted polymer chains (Fig. 1). On short lag times t, the MSDs exhibit power-law scaling $g_i(t) \propto t^{\alpha}$ with $\alpha \approx 2/3$, consistent with experimental observations for NP-grafted polymers in solution.[45] This power-law behavior emerges because the monomers along the polymer chain are hydrodynamically coupled and follow standard Zimm relaxations.[18] Over long t, g_i saturates at a finite value that increases with monomer index i. This saturation value is associated with the maximum displacement of the monomers due to the grafting constraint, and it depends on their position along the chain contour, indicated by the index i. Thus, the increase in saturation value with the index i reflects the increasing magnitude of positional fluctuations accessible to monomers farther from the grafting site on the NP surface.[63] Over intermediate time scales, however, we observe the emergence of an intermediate plateau for low monomer indices (*i.e.*, those close to the surface) that gradually disappears as i increases. These intermediate plateaus are consistent with experimental observations, where the plateau was attributed to confinement by neighboring chains.[44,45] The intermediate slowing of the dynamics is also reminiscent of those observed in supercooled colloidal liquids, where it is attributed to transient caging of a particle by its neighbors.[64–67] We thus attribute these plateaus to a confinement of grafted chains near the NP surface that weakens farther away. As discussed below, we test this hypothesis by characterizing the range of monomers that exhibit intermediate plateaus as a function of grafting density.

To examine the (potential) anisotropy of the chain relaxations, we decomposed the total MSD into components perpendicular and parallel to the NP surface (Fig. 1(b,c)). Broadly, the component MSDs exhibit qualitatively similar behavior as the total MSDs, with power-law scalings at short time scales, long-time plateaus, and intermediate plateaus for low-index monomers. Quantitatively, the saturation value for $g_{i,\perp}$ decreases as the grafting density γ increases due to excluded volume interactions that stretch and effectively stiffen the chain, resulting in greater localization of the monomers in the perpendicular direction. By contrast, the saturation value for $g_{i,\parallel}$ is largely insensitive to grafting density. This insensitivity may reflect the competing effects of decreased positional fluctuations but larger average radial positions (Supporting Information, Fig. S2) as the chains extend to accommodate the increased monomer density. These observations are consistent with previous LD simulation studies of semidilute spherical brushes,[39] as well as scaling theories for planar and cylindrical geometries[68] that predict that long-time-scale fluctuations normal to the grafting surface are more strongly influenced by γ than those in the lateral direction.

Following the methodology of previous studies,[39] we defined an effective relaxation time τ as the time at which the MSD reaches two-thirds of its saturation value $g_i(\tau) = (2/3)g_i(t \to \infty)$. Although the saturation value of $g_{i,\perp}$ monotonically increases with monomer index, the relaxation time in the perpendicular direction $\tau_{\perp}$ is non-monotonic (Fig. 2). The relaxation time initially increases with monomer index, as predicted by theory, but then passes through a maximum near the middle of the chain and decreases at higher monomer indices. This decrease in relaxation time occurs because the local monomer concentration decreases with increasing distance from the NP surface, and hence the motions of the chain segments further from the surface are less hindered by collisions with other chains.[39] Relaxation of these segments is also facilitated by their proximity to the free chain ends, which are bonded to only one neighbor and hence relax faster. The relaxation time in the

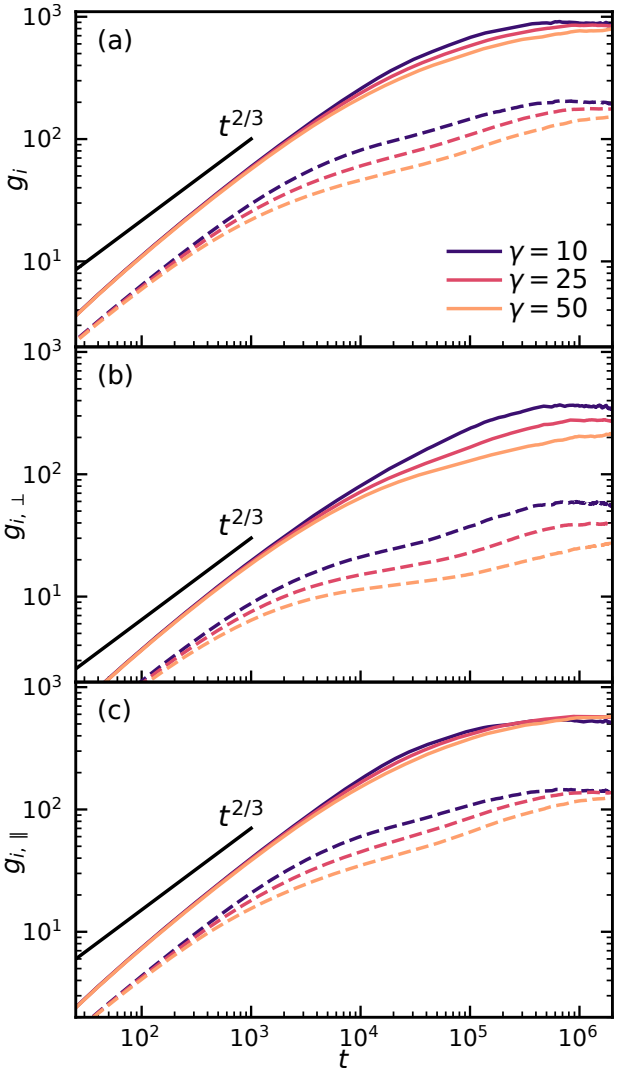

Figure 1. Mean-squared displacements (MSDs) g_i of monomers with indices $i = 40$ (dashed lines) and $i = 120$ (continuous lines) computed from hybrid MD–MPCD simulations for three reduced grafting densities γ. The panels show (a) the total MSD and the components (b) perpendicular and (c) parallel to the NP surface. The black lines show the early-time $t^{2/3}$ scaling behavior predicted by the Zimm model for systems with hydrodynamic interactions.

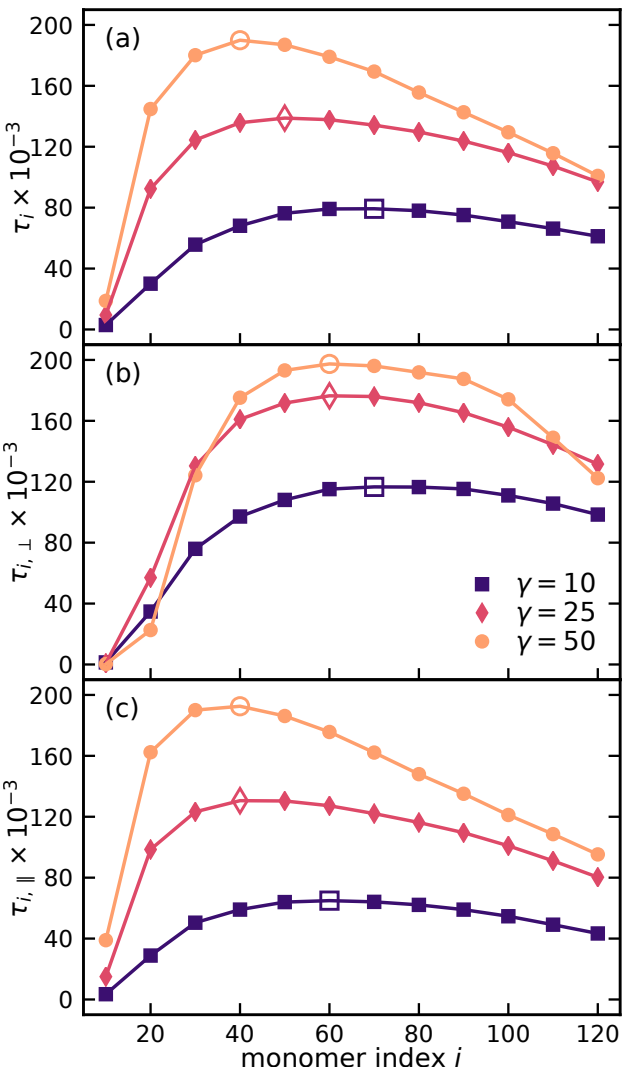

Figure 2. Relaxation times τ from hybrid MD–MPCD simulations as functions of monomer index i computed from (a) the total MSD and the components (b) perpendicular and (c) parallel to the NP surface. Open symbols identify maxima.

lateral direction $\tau_\parallel$ exhibits similar non-monotonic behavior, but the maximum is shifted to lower monomer indices, suggesting that relaxations in the parallel direction are more sensitive to their proximity to chain ends than those in the perpendicular direction. As expected, both $\tau_\perp$ and $\tau_\parallel$ increase with grafting density due to enhanced interactions with neighboring chains. Additionally, the position of the relaxation-time maximum shifts to lower monomer indices with increasing γ and is more pronounced for the parallel direction. This result indicates that the relaxations of monomers near the particle surface are more strongly hindered at higher grafting densities.

While these hindered dynamics are consistent with our hypothesis that grafted chains are confined, we directly tested this confinement picture by analyzing the intermediate plateaus. Specifically, we fitted the logarithm of the MSD to a cubic polynomial near the intermediate plateau, which allowed us to precisely quantify this plateau according to the inflection point of the polynomial. The associated time scale t_c was obtained from the root of the polynomial's second derivative, and the confinement length scale was estimated via $l_c = g_i(t_c)^{1/2}$ (Supporting Information, Fig. S3). We focus our analysis on dynamics in the parallel direction, which directly captures interactions between neighboring chains and removes complicating effects introduced by changes to chain conformation and the radial distribution of monomers. From this analysis, we find that both l_c and t_c increase monotonically with monomer index (Fig. 3). This increase indicates that monomers farther from the NP surface can move over longer distances (and commensurately, need longer times) before becoming confined. Additionally, both l_c and t_c decrease as the grafting density γ increases, consistent with stronger confinement at higher monomer densities. These trends imply that the chain dynamics are more strongly confined near the NP surface and at higher grafting densities. Comparison of t_c and $\tau_\parallel$ reveals that the two time scales are not strongly correlated (Supporting Information, Fig. S4), which is expected because they are associated with distinct physical processes and vary differently with monomer index and grafting density.

The inflection point of the fitted polynomial vanishes be-

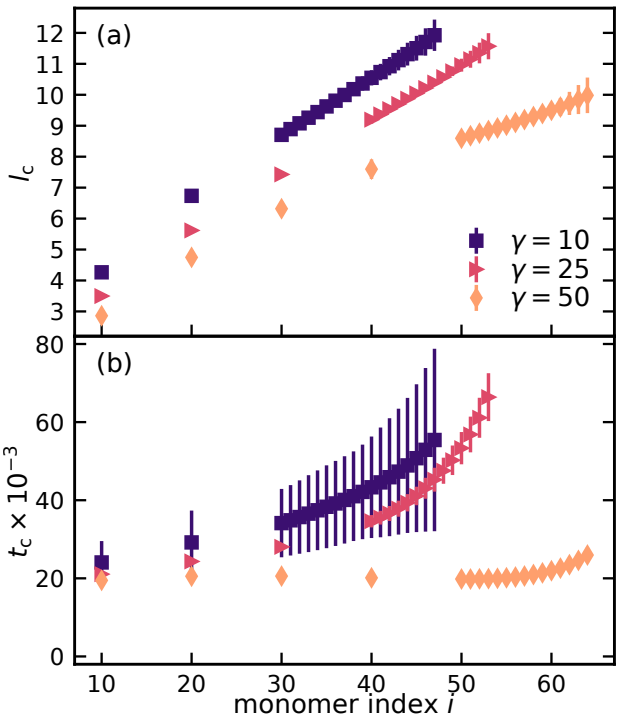

Figure 3. (a) Confinement length scale l_c and (b) associated time scale t_c computed from hybrid MD–MPCD simulations as a function of monomer index i.

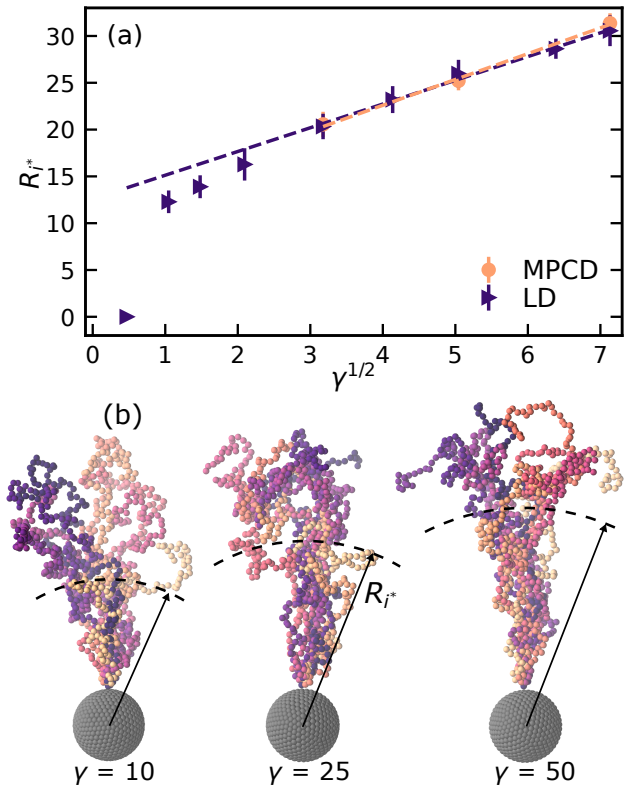

Figure 4. (a) Scaling behavior of R_{i*} with $\gamma^{1/2}$. R_{i*} is the average distance of monomer i^* from the NP's center, where i^* denotes the largest monomer index for which an intermediate-time inflection point is observed in the MSD. Symbols show data from the hybrid MD-MPCD and LD simulations (circles and triangles, respectively), and the dashed lines are linear fits indicating $R_{i*} \sim \gamma^{1/2}$ scaling. (b) Schematic showing the critical radius R_{i*} below which monomers exhibit confined dynamics at various grafting densities. At each grafting density, 10 different configurations sampled by a single, selected chain over a duration $\sim t_c$ are rendered. The orange-to-purple (light-to-dark) color scale signifies the chronological order of the sampled chain configurations.

yond a critical monomer index i^* that increases with increasing grafting density, suggesting that the intermediate chain dynamics are no longer strongly confined beyond the associated length and time scales l_c and t_c, respectively. According to Ohno et al.'s[34] extension of Daoud–Cotton theory,[32] the transition between the CPB and SDPB regimes occurs at a critical radius from the NP's center $R_{\mathrm{CPB}} = R_{\mathrm{NP}} b^2 R_{\mathrm{g},0}^{-2} \tilde{\nu}^{-1} \gamma^{1/2}$, where R_{NP} is the NP radius, b is the (effective) bond length, and $\tilde{\nu} = \nu/\sqrt{4\pi}$ is a rescaled excluded volume parameter. To compare the dynamical confinement to this model, we identified the critical monomer index i^* for each grafting density and computed its average distance from the NP's center R_{i*}. In qualitative agreement with this theoretical model, we find that R_{i*} exhibits the predicted dependence on grafting density and increases as $R_{i*} \sim \gamma^{1/2}$ (Fig. 4). Further, assuming $b = 1.28$ for Kremer–Grest chains,[35,69] we estimate that $\tilde{\nu} = 0.28$ from the slope of a linear fit to the data. This effective $\tilde{\nu}$ is close to the value $\tilde{\nu} = 0.30$ estimated from experiments[34] and simulations,[48] and it suggests that the chains are strongly stretched on length scales below R_{i*} due to the confinement imposed by their neighbors. Hence, our results indicate that the observed inflection in the MSDs is indicative of confined chain dynamics near the NP surface, and its presence delineates between the CPB- and SDPB-like regimes predicted by theory.

Complementary LD simulations (without HI) reveal remarkably similar behavior to the hybrid MD–MPCD simulations (with HI) performed at the same grafting densities. Indeed, the LD simulations exhibit intermediate time plateaus in the MSDs (Fig. 1; Supporting Information, Fig. S5) and similar long-time relaxation behavior (Fig. 2; Supporting Information, Fig. S6). The magnitude of R_{i*} and its scaling behavior at large grafting densities ($\gamma^{1/2} > 3$) from the two models are nearly indistinguishable (Fig. 4). Thus, the confined dynamics in the CPB regime and the transition to SDPB-like behavior do not appear to be strongly influenced by HI, consistent with earlier investigations of free polymers in solution that found that HI are screened at high monomer densities.[70] Interestingly, extrapolation of a linear fit to R_{i*} for $\gamma^{1/2} > 3$ yields a positive intercept (i.e., $R_{i*} > 0$ at $\gamma^{1/2} = 0$), at odds with theoretical expectations. To investigate this possibility, we performed additional LD simulations at lower grafting densities. We observe that R_{i*} deviates from the $\gamma^{1/2}$ scaling behavior for $\gamma^{1/2} \lesssim 2$ (Fig. 4). In the limit of a single polymer chain grafted to the NP, the inflection point in the MSDs vanishes completely for all monomers and no evidence of confined dynamics is observed (Supporting Information, Fig. S7), suggesting that R_{i*} is effectively zero (Fig. 4). Thus, the LD simulations predict $R_{i*} \to 0$ and deviations from $\gamma^{1/2}$ scaling at sufficiently low grafting densities.

In summary, our simulations of spherical polymer brushes in solution demonstrate that chain segments near the grafting surface exhibit an intermediate plateau in their MSDs, consistent with the confined dynamics reported in NSE experiments.[44,45] By analyzing the intermediate plateaus, we identified the characteristic length scale beyond which the confined dynamics vanish. The variation of this length scale with grafting density is in agreement with that predicted by

the extended Daoud–Cotton model[32] of Ohno et al.[34] for the critical radius associated with the transition from a concentrated to a semidilute polymer brush. While preparing our manuscript, a recent study was published on the dynamics and structure of chains in spherical polymer brushes under melt-like conditions.[48] Using the theory of Ohno et al.[34] for solutions, they estimated the critical radius for the CPB regime and demonstrated that the grafted chains exhibit stretched conformations and slow segmental dynamics below this length scale. Although those observations are consistent with our findings for polymer-grafted NPs in solution, our analysis reveals a hitherto unreported dynamical length scale that behaves similarly to the hypothesized critical radius of the extended Daoud–Cotton model. Thus, we independently validate the extended Daoud–Cotton model and connect dynamical and static fluctuations in spherical polymer brushes.

Acknowledgement We thank the National Science Foundation (CBET-2004652, to JCC and JCP, CBET-1751173, to JCP, and CBET-2223084, to MPH) and the Welch Foundation (E-1869, to JCC, and E-1882, to JCP) for support of this work. RPS acknowledges support from ACS Petroleum Research Fund Doctoral New Investigator grant 65826-DNI9. AN acknowledges support by the Deutsche Forschungsgemeinschaft (DFG, German Research Foundation) through Project No. 470113688. Computational resources were generously provided by the Hewlett Packard Enterprise Data Science Institute at the University of Houston and the Texas Advanced Computing Center at the University of Texas at Austin.

Supporting Information Available

Detailed computational methods, additional simulation data, and example analyses.

References

(1) Akcora, P.; Liu, H.; Kumar, S. K.; Moll, J.; Li, Y.; Benicewicz, B. C.; Schadler, L. S.; Acehan, D.; Panagiotopoulos, A. Z.; Pryamitsyn, V.; Ganesan, V.; Ilavsky, J.; Thiyagarajan, P.; Colby, R. H.; Douglas, J. F. Anisotropic self-assembly of spherical polymer-grafted nanoparticles. *Nat. Mat.* **2009**, *8*, 354–359.

(2) Chevigny, C. C.; Dalmas, F.; Di Cola, E.; Gigmes, D.; Bertin, D.; Boué, F.; Jestin, J.; Boué, F.; Jestin, J. Polymer-Grafted-Nanoparticles Nanocomposites: Dispersion, Grafted Chain Conformation, and Rheological Behavior. *Macromolecules* **2011**, *44*, 122–133.

(3) Martin, T. B.; Mongcopa, K. I. S.; Ashkar, R.; Butler, P.; Krishnamoorti, R.; Jayaraman, A. Wetting–Dewetting and Dispersion–Aggregation Transitions Are Distinct for Polymer Grafted Nanoparticles in Chemically Dissimilar Polymer Matrix. *J. Am. Chem. Soc.* **2015**, *137*, 10624–10631.

(4) Kulshreshtha, A.; Jayaraman, A. Dispersion and Aggregation of Polymer Grafted Particles in Polymer Nanocomposites Driven by the Hardness and Size of the Grafted Layer Tuned by Attractive Graft–Matrix Interactions. *Macromolecules* **2020**, *53*, 1302–1313.

(5) Bilchak, C. R.; Jhalaria, M.; Huang, Y.; Abbas, Z.; Midya, J.; Benedetti, F. M.; Parisi, D.; Egger, W.; Dickmann, M.; Minelli, M.; Doghieri, F.; Nikoubashman, A.; Durning, C. J.; Vlassopoulos, D.; Jestin, J.; Smith, Z. P.; Benicewicz, B. C.; Rubinstein, M.; Leibler, L.; Kumar, S. K. Tuning selectivities in gas separation membranes based on polymer-grafted nanoparticles. *ACS Nano* **2020**, *14*, 17174–17183.

(6) Liu, G.; Cai, M.; Zhou, F.; Liu, W. Charged Polymer Brushes-Grafted Hollow Silica Nanoparticles as a Novel Promising Material for Simultaneous Joint Lubrication and Treatment. *J. Phys. Chem. B.* **2014**, *118*, 4920–4931.

(7) Mocny, P.; Klok, H.-A. Tribology of Surface-Grafted Polymer Brushes. *Mol. Syst. Des. Eng.* **2016**, *1*, 141–154.

(8) Gref, R.; Minamitake, Y.; Peracchia, M. T.; Trubetskoy, V.; Torchilin, V.; Langer, R. Biodegradable Long-Circulating Polymeric Nanospheres. *Science* **1994**, *263*, 1600–1603.

(9) Farokhzad, O. C.; Cheng, J.; Teply, B. A.; Sherifi, I.; Jon, S.; Kantoff, P. W.; Richie, J. P.; Langer, R. Targeted Nanoparticle-Aptamer Bioconjugates for Cancer Chemotherapy in Vivo. *Proc. Natl. Acad. Sci. U. S. A.* **2006**, *103*, 6315–20.

(10) Nance, E. A.; Woodworth, G. F.; Sailor, K. A.; Shih, T.-Y.; Xu, Q.; Swaminathan, G.; Xiang, D.; Eberhart, C.; Hanes, J. A Dense Poly(Ethylene Glycol) Coating Improves Penetration of Large Polymeric Nanoparticles Within Brain Tissue. *Sci. Transl. Med.* **2012**, *4*.

(11) Pan, A.; Jakaria, M. G.; Meenach, S. A.; Bothun, G. D. Radiofrequency and Near-Infrared Responsive Core-Shell Nanostructures Using Layersome Templates for Cancer Treatment. *ACS Appl. Bio Mater.* **2020**, *3*, 273–281.

(12) Rowe, M. D.; Chang, C.-C.; Thamm, D. H.; Kraft, S. L.; Harmon, J. F. J.; Vogt, A. P.; Sumerlin, B. S.; Boyes, S. G. Tuning the Magnetic Resonance Imaging Properties of Positive Contrast Agent Nanoparticles by Surface Modification with RAFT Polymers. *Langmuir* **2009**, *25*, 9487–9499.

(13) Song, J.; Pu, L.; Zhou, J.; Duan, B.; Duan, H. Biodegradable Theranostic Plasmonic Vesicles of Amphiphilic Gold Nanorods. *ACS Nano* **2013**, *7*, 9947–9960.

(14) Black, K. C. L.; Wang, Y.; Luehmann, H. P.; Cai, X.; Xing, W.; Pang, B.; Zhao, Y.; Cutler, C. S.; Wang, L. V.; Liu, Y.; Xia, Y. Radioactive ^{198}Au-doped Nanostructures with Different Shapes for in Vivo Analyses of Their Biodistribution, Tumor Uptake, and Intratumoral Distribution. *ACS Nano* **2014**, *8*, 4385–4394.

(15) Long, D.; Ajdari, A.; Leibler, L. How Do Grafted Polymer Layers Alter the Dynamics of Wetting? *Langmuir* **1996**, *12*, 1675–1680.

(16) Senaratne, W.; Andruzzi, L.; Ober, C. K. Self-Assembled Monolayers and Polymer Brushes in Biotechnology: Current Applications and Future Perspectives. *Biomacromolecules* **2005**, *6*, 2427–2448.

(17) Yadav, V.; Jaimes-Lizcano, Y. A.; Dewangan, N. K.; Park, N.; Li, T. H.; Robertson, M. L.; Conrad, J. C. Tuning Bacterial Attachment and Detachment via the Thickness and Dispersity of a pH-Responsive Polymer Brush. *ACS Appl. Mater. Interfaces* **2017**, *9*, 44900–44910.

(18) Rubinstein, M.; Colby, R. H. *Polymer Physics*; Oxford University Press: New York, 2003.

(19) Alexander, S. Adsorption of chain molecules with a polar head: A scaling description. *J. Phys. (Paris)* **1977**, *38*, 983–987.

(20) de Gennes, P. G. Conformations of Polymers Attached to an Interface. *Macromolecules* **1980**, *13*, 1069–1075.

(21) Zhulina, E. B.; Borisov, O. V.; Priamitsyn, V. A. Theory of Steric Stabilization of Colloid Dispersions by Grafted Polymers. *J. Colloid Interface Sci.* **1990**, *137*, 495–511.

(22) Milner, S. T. Polymer Brushes. *Science* **1991**, *251*, 905–914.

(23) Karim, A.; Satija, S. K.; Douglas, J. F.; Ankner, J. F.; Fetters, L. J. Neutron Reflectivity Study of the Density Profile of a Model End-Grafted Polymer Brush: Influence of Solvent Quality. *Phys. Rev. Lett.* **1994**, *73*, 3407–3410.

(24) Aoki, H.; Kitamura, M.; Ito, S. Nanosecond Dynamics of Poly(Methyl Methacrylate) Brushes in Solvents Studied by Fluorescence Depolarization Method. *Macromolecules* **2008**, *41*, 285–287.

(25) Gianneli, M.; Roskamp, R. F.; Jonas, U.; Loppinet, B.; Fytas, G.; Knoll, W. Dynamics of Swollen Gel Layers Anchored to Solid Surfaces. *Soft Matter* **2008**, *4*, 1443.

(26) de Gennes, P.-G. Dynamics of a Diffuse Layer of Adsorbed Polymer. *C. R. Acad. Sci. Paris. Ser. II* **1986**, *302*, 765–768.

(27) de Gennes, P. G. Polymers at an Interface; a Simplified View. *Adv. Colloid Interface Sci.* **1987**, *27*, 189–209.

(28) Farago, B.; Monkenbusch, M.; Richter, D.; Huang, J. S.; Fetters, L. J.; Gast, A. P. Collective Dynamics of Tethered Chains: Breathing Modes. *Phys. Rev. Lett.* **1993**, *71*, 1015–1018.

(29) Yakubov, G. E.; Loppinet, B.; Zhang, H.; Rühe, J.; Sigel, R.; Fytas, G. Collective Dynamics of an End-Grafted Polymer Brush in Solvents of Varying Quality. *Phys. Rev. Lett.* **2004**, *92*, 115501.

(30) Koga, T.; Barkley, D.; Nagao, M.; Taniguchi, T.; Carrillo, J.-M. Y.; Sumpter, B. G.; Masui, T.; Kishimoto, H.; Koga, M.; Rudick, J. G.; Endoh, M. K. Interphase Structures and Dynamics near Nanofiller Surfaces in Polymer Solutions. *Macromolecules* **2018**, *51*, 9462–9470.

(31) Semenov, A. N.; Anastasiadis, S. H. Collective Dynamics of Polymer Brushes. *Macromolecules* **2000**, *33*, 613–623.

(32) Daoud, M.; Cotton, J. Star shaped polymers : a model for the conformation and its concentration dependence. *Journal de physique.* **1982**, *43*.

(33) Förster, S.; Wenz, E.; Lindner, P. Density Profile of Spherical Polymer Brushes. *Phys. Rev. Lett.* **1996**, *77*, 95.

(34) Ohno, K.; Morinaga, T.; Takeno, S.; Tsujii, Y.; Fukuda, T. Suspensions of Silica Particles Grafted with Concentrated Polymer Brush: Effects of Graft Chain Length on Brush Layer Thickness and Colloidal Crystallization. *Macromolecules* **2007**, *40*, 9143–9150.

(35) Midya, J.; Rubinstein, M.; Kumar, S. K.; Nikoubashman, A. Structure of Polymer-Grafted Nanoparticle Melts. *ACS Nano* **2020**, *14*, 15505–15516.

(36) Wijmans, C. M.; Zhulina, E. B. Polymer Brushes at Curved

Surfaces. *Macromolecules* **1993**, *26*, 7214–7224.
(37) Dukes, D.; Li, Y.; Lewis, S.; Benicewicz, B.; Schadler, L.; Kumar, S. K. Conformational Transitions of Spherical Polymer Brushes: Synthesis, Characterization, and Theory. *Macromolecules* **2010**, *43*, 1564–1570.
(38) Hore, M. J. A.; Ford, J.; Ohno, K.; Composto, R. J.; Hammouda, B. Direct Measurements of Polymer Brush Conformation Using Small-Angle Neutron Scattering (SANS) from Highly Grafted Iron Oxide Nanoparticles in Homopolymer Melts. *Macromolecules* **2013**, *46*, 9341–9348.
(39) Lo Verso, F.; Yelash, L.; Binder, K. Dynamics of Macromolecules Grafted in Spherical Brushes under Good Solvent Conditions. *Macromolecules* **2013**, *46*, 4716–4722.
(40) Li, T.-H.; Yadav, V.; Conrad, J. C.; Robertson, M. L. Effect of Dispersity on the Conformation of Spherical Polymer Brushes. *ACS Macro Lett.* **2021**, *10*, 518–524.
(41) Klushin, L. I.; Skvortsov, A. M. Critical Dynamics of a Polymer Chain in a Grafted Monolayer. *Macromolecules* **1991**, *24*, 1549–1553.
(42) Lang, M.; Werner, M.; Dockhorn, R.; Kreer, T. Arm Retraction Dynamics in Dense Polymer Brushes. *Macromolecules* **2016**, *49*, 5190–5201.
(43) Reith, D.; Milchev, A.; Virnau, P.; Binder, K. Computer Simulation Studies of Chain Dynamics in Polymer Brushes. *Macromolecules* **2012**, *45*, 4381–4393.
(44) Mark, C.; Holderer, O.; Allgaier, J.; Hübner, E.; Pyckhout-Hintzen, W.; Zamponi, M.; Radulescu, A.; Feoktystov, A.; Monkenbusch, M.; Jalarvo, N.; Richter, D. Polymer Chain Conformation and Dynamical Confinement in a Model One-Component Nanocomposite. *Phys. Rev. Lett.* **2017**, *119*, 047801.
(45) Poling-Skutvik, R.; Olafson, K. N.; Narayanan, S.; Stingaciu, L.; Faraone, A.; Conrad, J. C.; Krishnamoorti, R. Confined Dynamics of Grafted Polymer Chains in Solutions of Linear Polymer. *Macromolecules* **2017**, *50*, 7372–7379.
(46) Wei, Y.; Xu, Y.; Faraone, A.; Hore, M. J. Local Structure and Relaxation Dynamics in the Brush of Polymer-Grafted Silica Nanoparticles. *ACS Macro Letters* **2018**, *7*, 699–704.
(47) Miller, C. A.; Hore, M. J. A. Simulation of the Coronal Dynamics of Polymer-Grafted Nanoparticles. *ACS Polym. Au* **2022**, *2*, 157–168.
(48) Wei, Y.; Chen, Q.; Zhao, H.; Duan, P.; Zhang, L.; Liu, J. Conformation and Dynamics along the Chain Contours of Polymer-Grafted Nanoparticles. *Langmuir* **2023**, *39*, 11003–11015.
(49) Grest, G. S.; Kremer, K. Molecular dynamics simulation for polymers in the presence of a heat bath. *Phys. Rev. A* **1986**, *33*, 3628.
(50) Kapral, R. Multiparticle collision dynamics: simulation of complex systems on mesoscales. *Adv. Chem. Phys.* **2008**, *140*, 89.
(51) Gompper, G.; Ihle, T.; Kroll, D.; Winkler, R. G. Multi-particle collision dynamics: A particle-based mesoscale simulation approach to the hydrodynamics of complex fluids. *Adv. Polym. Sci.* **2009**, *221*, 1–87.
(52) Chen, R.; Poling-Skutvik, R.; Nikoubashman, A.; Howard, M. P.; Conrad, J. C.; Palmer, J. C. Coupling of nanoparticle dynamics to polymer center-of-mass motion in semidilute polymer solutions. *Macromolecules* **2018**, *51*, 1865–1872.
(53) Chen, R.; Poling-Skutvik, R.; Howard, M. P.; Nikoubashman, A.; Egorov, S. A.; Conrad, J. C.; Palmer, J. C. Influence of polymer flexibility on nanoparticle dynamics in semidilute solutions. *Soft Matter* **2019**, *15*, 1260–1268.
(54) Howard, M. P.; Nikoubashman, A.; Palmer, J. C. Modeling hydrodynamic interactions in soft materials with multiparticle collision dynamics. *Curr. Opin. Chem. Eng.* **2019**, *23*, 34.
(55) Chen, R.; Kotkar, S. B.; Poling-Skutvik, R.; Howard, M. P.; Nikoubashman, A.; Conrad, J. C.; Palmer, J. C. Nanoparticle dynamics in semidilute polymer solutions: Rings versus linear chains. *Journal of Rheology* **2021**, *65*, 745–755.
(56) Poblete, S.; Wysocki, A.; Gompper, G.; Winkler, R. G. Hydrodynamics of discrete-particle models of spherical colloids: A multiparticle collision dynamics simulation study. *Phys. Rev. E* **2014**, *90*, 033314.
(57) Wani, Y. M.; Kovakas, P. G.; Nikoubashman, A.; Howard, M. P. Diffusion and sedimentation in colloidal suspensions using multiparticle collision dynamics with a discrete particle model. *The Journal of Chemical Physics* **2022**, *156*, 024901.
(58) Bishop, M.; Kalos, M. H.; Frisch, H. L. Molecular dynamics of polymeric systems. *J. Chem. Phys.* **1979**, *70*, 1299–1304.
(59) Weeks, J. D.; Chandler, D.; Andersen, H. C. Role of repulsive forces in determining the equilibrium structure of simple liquids. *J. Chem. Phys.* **1971**, *54*, 5237–5247.
(60) Allahyarov, E.; Gompper, G. Mesoscopic solvent simulations: Multiparticle-collision dynamics of three-dimensional flows. *Phys. Rev. E* **2002**, *66*, 36702.
(61) Noguchi, H.; Kikuchi, N.; Gompper, G. Particle-based mesoscale hydrodynamic techniques. *EPL (Europhysics Lett.)* **2007**, *78*, 10005.
(62) Huang, C.-C. C.; Winkler, R. G.; Sutmann, G.; Gompper, G. Semidilute polymer solutions at equilibrium and under shear flow. *Macromolecules* **2010**, *43*, 10107–10116.
(63) Bickel, T. A note on confined diffusion. *Physica A Stat. Mech. Appl.* **2007**, *377*, 24–32.
(64) Van Megen, W.; Underwood, S. M. Dynamic-Light-Scattering Study of Glasses of Hard Colloidal Spheres. *Phys. Rev. E* **1993**, *47*, 248–261.
(65) Kob, W.; Donati, C.; Plimpton, S. J.; Poole, P. H.; Glotzer, S. C. Dynamical Heterogeneities in a Supercooled Lennard-Jones Liquid. *Phys. Rev. Lett.* **1997**, *79*, 2827–2830.
(66) Roberts, R. C.; Poling-Skutvik, R.; Palmer, J. C.; Conrad, J. C. Tracer Transport Probes Relaxation and Structure of Attractive and Repulsive Glassy Liquids. *The Journal of Physical Chemistry Letters* **2018**, *9*, 3008–3013.
(67) Roberts, R. C.; Poling-Skutvik, R.; Conrad, J. C.; Palmer, J. C. Tracer transport in attractive and repulsive supercooled liquids and glasses. *The Journal of Chemical Physics* **2019**, *151*, 194501.
(68) Binder, K.; Milchev, A. Polymer brushes on flat and curved surfaces: How computer simulations can help to test theories and to interpret experiments. *Journal of Polymer Science Part B: Polymer Physics* **2012**, *50*, 1515–1555.
(69) Chremos, A.; Nikoubashman, A.; Panagiotopoulos, A. Z. Flory-Huggins parameter χ, from binary mixtures of Lennard-Jones particles to block copolymer melts. *The Journal of Chemical Physics* **2014**, *140*, 054909.
(70) Richter, D.; Hayter, J. B.; Mezei, F.; Ewen, B. Dynamical Scaling in Polymer Solutions Investigated by the Neutron Spin-Echo Technique. *Phys. Rev. Lett.* **1978**, *41*, 1484–1487.

TOC Graphic

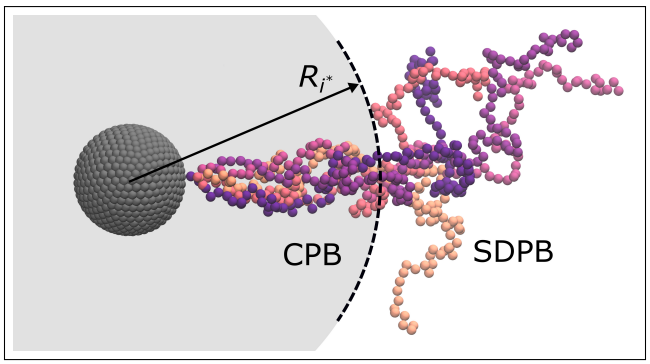

Supporting Information: Confined dynamics in spherical polymer brushes

Shivraj B. Kotkar,[†] Michael P. Howard,[‡] Arash Nikoubashman,[¶,§] Jacinta C. Conrad,[*,†] Ryan Poling-Skutvik,[*,‖] and Jeremy C. Palmer[*,†]

†*Department of Chemical and Biomolecular Engineering, University of Houston, Houston, TX 77204*

‡*Department of Chemical Engineering, Auburn University, Auburn, AL 36849*

¶*Leibniz-Institut für Polymerforschung Dresden e.V., Hohe Straße 6, 01069 Dresden, Germany*

§*Institut für Theoretische Physik, Technische Universität Dresden, 01069 Dresden, Germany*

‖*Department of Chemical Engineering, University of Rhode Island, Kingston, RI 02881*

E-mail: jcconrad@uh.edu; ryanps@uri.edu; jcpalmer@uh.edu

1 Polymer brush model

Following the main text, the model parameters and physical quantities from the simulations are reported using fundamental units of a, m, ε, and $\tilde{t} = \sqrt{ma^2/\varepsilon}$ for length, mass, energy, and time, respectively. The polymer brushes were modeled as N_c chains grafted to the surface of a spherical nanoparticle (NP). Each polymer chain contained 120 monomers with diameter $a_\mathrm{P} = 1$ and mass $m_\mathrm{P} = 5.0$. The NP was modeled as a collection of monomer-sized beads

positioned at 642 vertices on the surface of a sphere of radius $R_{\mathrm{NP}} = 5$, yielding a surface density of ≈ 2.[S1,S2] The positions of the vertices were generated by recursively subdividing the faces of a regular icosahedron into equilateral triangles and then radially scaling the vertices to a distance R_{NP} from the center of the sphere. To achieve near-uniform grafting on the NP surface, we used Monte Carlo sampling and simulated annealing to solve the Thomson Problem on the 642 discrete vertices using N_{c} classical electrons.[S3] The polymer chains were end-grafted to the N_{c} vertices occupied by the electrons in the lowest energy configuration obtained from the Monte Carlo sampling. Spring-like bonds between adjacent monomers on the polymer chains and between the end monomers and grafting sites on the NP surface were modeled using the finite extensible nonlinear elastic (FENE) potential:[S4]

$$U_{\mathrm{FENE}}(r_{ij}) = \begin{cases} -\frac{1}{2} k {r_0}^2 \ln\left[1 - \dfrac{r_{ij}^2}{{r_0}^2}\right], & r_{ij} < r_0 \\ \infty, & r_{ij} \geq r_0 \end{cases}, \tag{S1}$$

where r_{ij} is the separation distance between particles i and j, $k = 30$ is the spring constant, and $r_0 = 1.5$ is the maximum bond extension length. Excluded volume interactions between particles were modeled use the Weeks-Chandler-Andersen (WCA) potential:[S5]

$$U_{\mathrm{WCA}}(r_{ij}) = \begin{cases} 4\left[\left(\dfrac{a_{ij}}{r_{ij}}\right)^{12} - \left(\dfrac{a_{ij}}{r_{ij}}\right)^{6}\right] + 1, & r_{ij} \leq 2^{1/6} a_{ij} \\ 0, & r_{ij} > 2^{1/6} a_{ij} \end{cases}, \tag{S2}$$

where $a_{ij} = a_{\mathrm{P}} = 1$ are the monomer–monomer and monomer–NP bead interactions.

2 Simulation protocol

Hybrid molecular dynamics and multi-particle collision dynamics (MD–MPCD) and Langevin dynamics (LD) simulations of the model polymer brushes were carried out using HOOMD-Blue 2.9.2.[S6,S7] All simulations were performed in a periodic, cubic box with edge length $L_{\mathrm{box}} = 130$ at a reduced temperature $T = 1$, and the equations of motion for the polymer beads were integrated using a velocity-Verlet scheme with a time step of 0.005 time units. The LD simulations were run for 10^7 time units, using a damping coefficient of 5.56.[S8] Polymer brush dynamics were analyzed using the second half of each trajectory, discarding the first half to ensure proper equilibration. The MD–MPCD trajectories were initiated from equilibrated brush configurations taken from the LD simulations and propagated for 2×10^6 time units. The hybrid MD–MPCD simulations were performed using a collision cell with an edge length of unity, a solvent particle mass $m_{\mathrm{s}} = 1$, an average solvent density $\rho = 5$ (5 solvent particles per collision cell), and a collision time step of 0.09 time units. Solvent collisions were handled using a momentum-conserving version of the Andersen thermostat,[S9,S10] and the reference positions of the cell were randomly shifted before each collision step to ensure Galilean invariance.[S11] These standard choices give yield an MPCD solvent with Schmidt number $\mathrm{Sc} \approx 12.0$ and dynamic viscosity $\eta_{\mathrm{s}} \approx 4.0$. The polymer monomers and NP beads were coupled to the MPCD solvent using the scheme in Ref. S12.

Hybrid MD–MPCD simulations were performed at three reduced grafting densities, $\gamma = \{10, 25, 50\}$. These values were chosen to fall within the range probed in recent experiments.[S13] Complementary LD simulations were performed over a broader range of grafting densities: $\gamma = \{0.22, 1.10, 2.19, 4.39, 10, 17, 25, 40, 50\}$. To obtain reliable statistics, the mean-squared displacements (MSDs) were averaged over monomers with the same index on different chains grafted to the NP. In each case, the monomer MSDs were computed by averaging over at least 30 polymer chains. At low γ, adhering to this criterion required averaging over multiple independent simulations performed at the same grafting density.

3 Mean-squared displacement decomposition

The total monomer MSD was decomposed to characterize chain dynamics in the directions perpendicular and parallel to the NP surface (Fig. S1). The perpendicular component $g_{i,\perp}$ was defined to be co-linear with the vector adjoining the NP's center of mass and the monomer's initial position at zero lag time $\mathbf{r}_i(0)$, whereas the parallel component $g_{i,\parallel}$ was orthogonal to the adjoining vector.

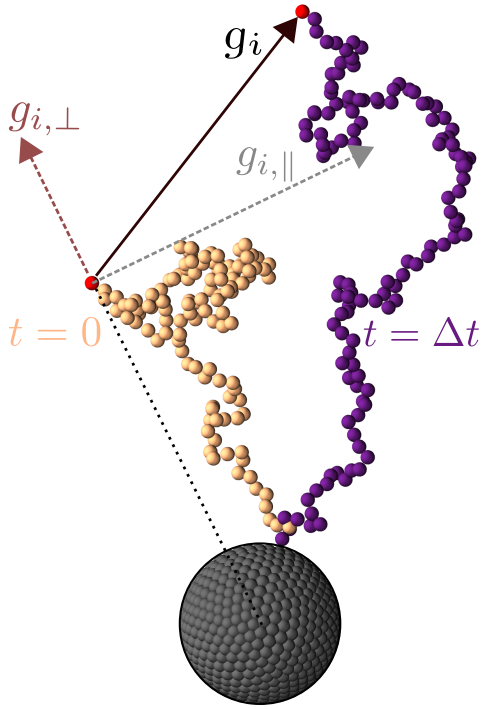

Figure S1: Decomposition of g_i into components that are perpendicular and parallel to the NP surface at lag time $t = 0$.

4 Monomer density profiles

To investigate the effects of grafting density on brush structure, the monomer number density profile was computed from the hybrid MD–MPCD simulations. As grafting density increases, the monomer density profiles broaden, indicating that the polymer chains become increasingly extended.[S14]

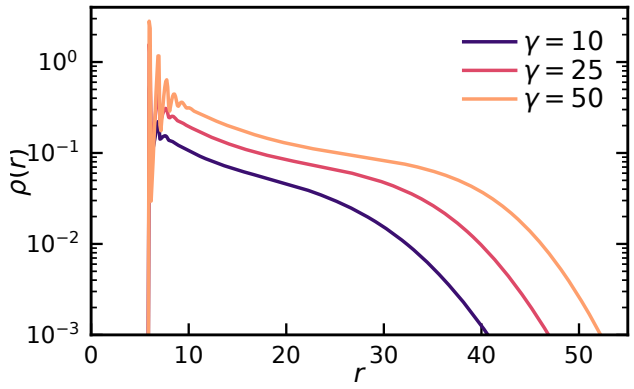

Figure S2: Monomer density profiles $\rho(r)$ as a function of the radial distance r from the center of mass of the NP computed from hybrid MD–MPCD simulations.

5 Analysis of the MSD inflection points

The inflection point in the monomer MSDs on intermediate time scales was characterized by fitting the logarithm of the MSD (y) as a function of the logarithm of t (x) using a cubic polynomial function, $y(x) = ax^3 + bx^2 + cx + d$ (Fig. S3(a)). In each case, we obtained excellent fits to the MSDs, with typical fit errors of fit error $= 100 \times |\text{Data} - \text{Fit}| \,/\, |\text{Data}|$ of less than 1% (Fig. S3 (b)). The time scale t_c associated with the inflection point was obtained from the root of the second derivative, and the confinement length was estimated from the square root of the MSD at t_c i.e., $l_c = \sqrt{g_i(t_c)}$ (Fig. S3(c)).

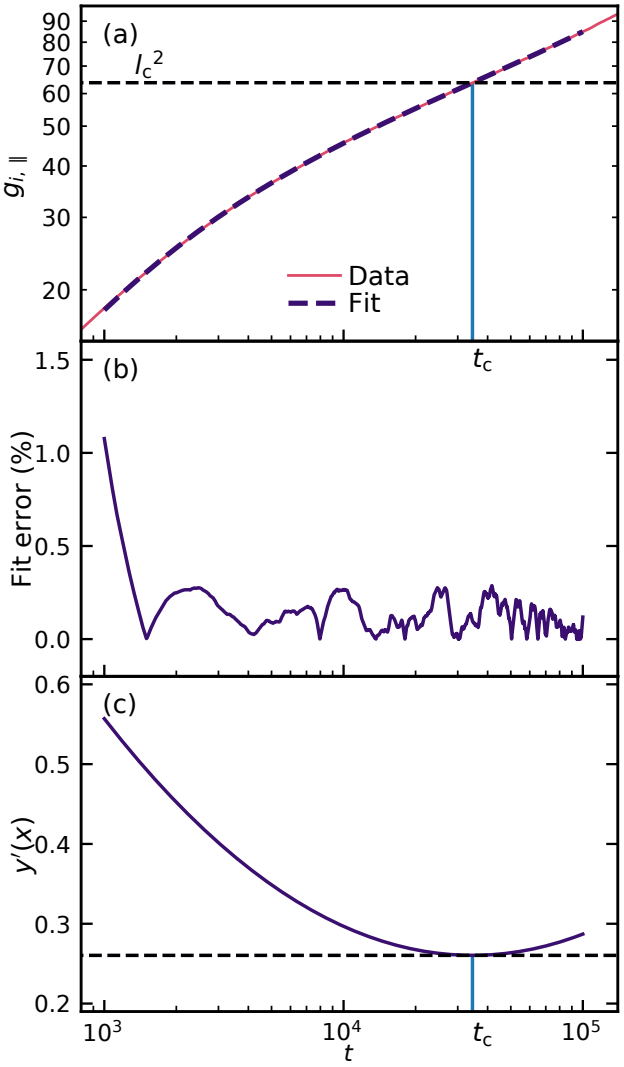

Figure S3: Example of the fitting procedure used to determine the time and length scales associated with the intermediate-time inflection point in the mean-squared displacements. (a) Mean-squared displacement parallel to the NP surface for monomer $i = 40$ at $\gamma = 25$. The dashed line is a fit to a cubic polynomial. (b) Percent fitting error for the example in (a). (c) The first derivative of the cubic polynomial fit function $y'(x)$ illustrating that t_c corresponds to a minimum in this function and a root of the second derivative.

6 Comparison relaxation time and inflection point time scale

Comparison of the relaxation time $\tau_{\|}$ and time scale associated with the intermediate-time inflection point τ_c reveal that the two are not strongly correlated. Indeed, no correlation is expected because $\tau_{\|}$ is associated with the long-time relaxation due to the grafting constraint at the NP surface, whereas τ_c characterizes the confinement arising from interactions with neighboring chains. Moreover, the long-time plateau associated with $\tau_{\|}$ exists for all monomers and is largely insensitive to grafting density, whereas the intermediate-time inflection point associated with τ_c completely vanishes at high monomer indices i and at sufficient low grafting densities due to the transition between CPB and SDPB regimes.

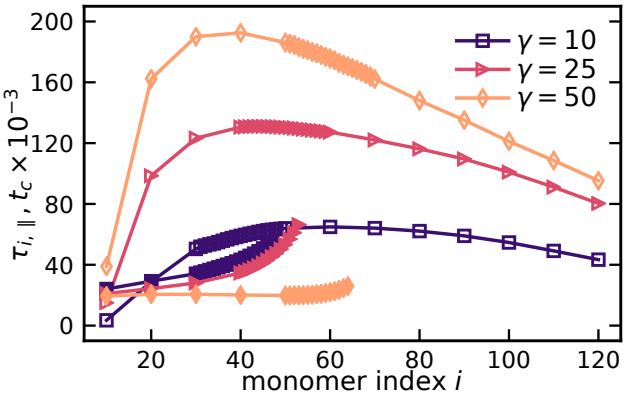

Figure S4: Comparison of the relaxation time $\tau_{\|}$ (open symbols) and time associated with the intermediate-time inflection point t_c (close symbols).

7 Results from LD simulations

Complementary LD simulations were performed to investigate the dynamics of spherical polymer brushes in the absence of hydrodynamic interactions (HI). The LD simulations (without HI) reveal remarkably similar behavior to the hybrid MD–MPCD simulations (with HI) performed at the same grafting densities. The LD simulations exhibit intermediate time plateaus in the monomer MSDs (Fig. S5) and similar long-time relaxation behavior (Fig. S6). Additionally, LD simulations were performed to investigate the limiting case of a a single polymer chain grafted to the NP. In this case, the inflection point in the MSDs vanishes completely for all monomers and no evidence of confined dynamics is observed (Fig. S7).

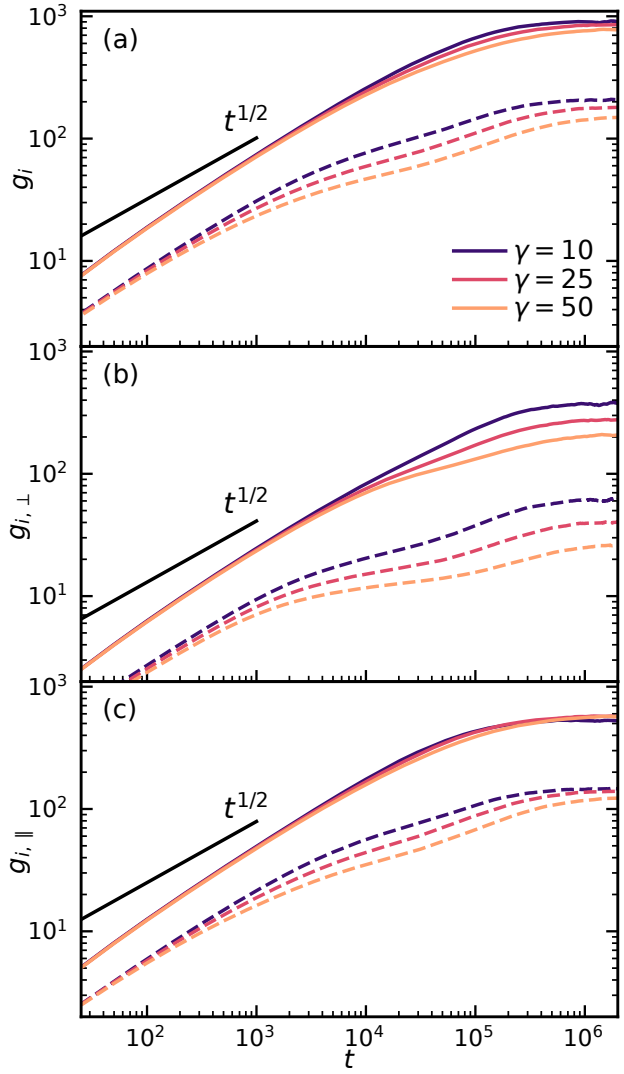

Figure S5: Mean-squared displacements of monomers with indices $i = 40$ (dashed line) and $i = 120$ (continuous line) computed from LD simulations. The panels show (a) the total MSD and the components (b) perpendicular and (c) parallel to the NP surface. The black lines show the early-time $t^{1/2}$ scaling behavior predicted by the Rouse model for systems without hydrodynamic interactions.

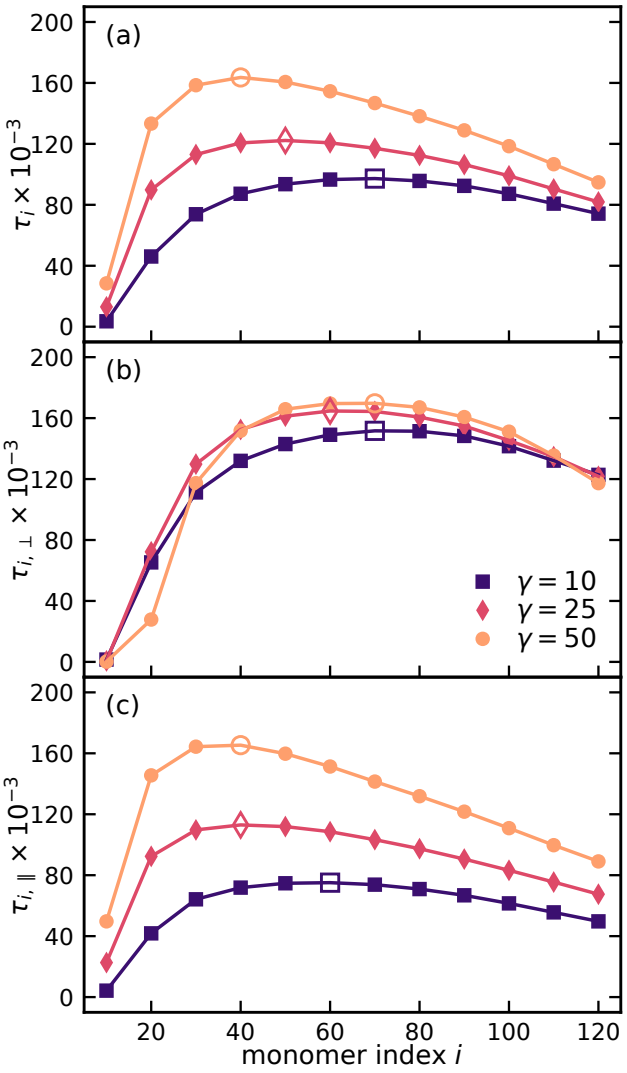

Figure S6: Relaxation time τ from LD simulations as a function of monomer index i computed from (a) the total MSD and the components (b) perpendicular and (c) parallel to the NP surface.

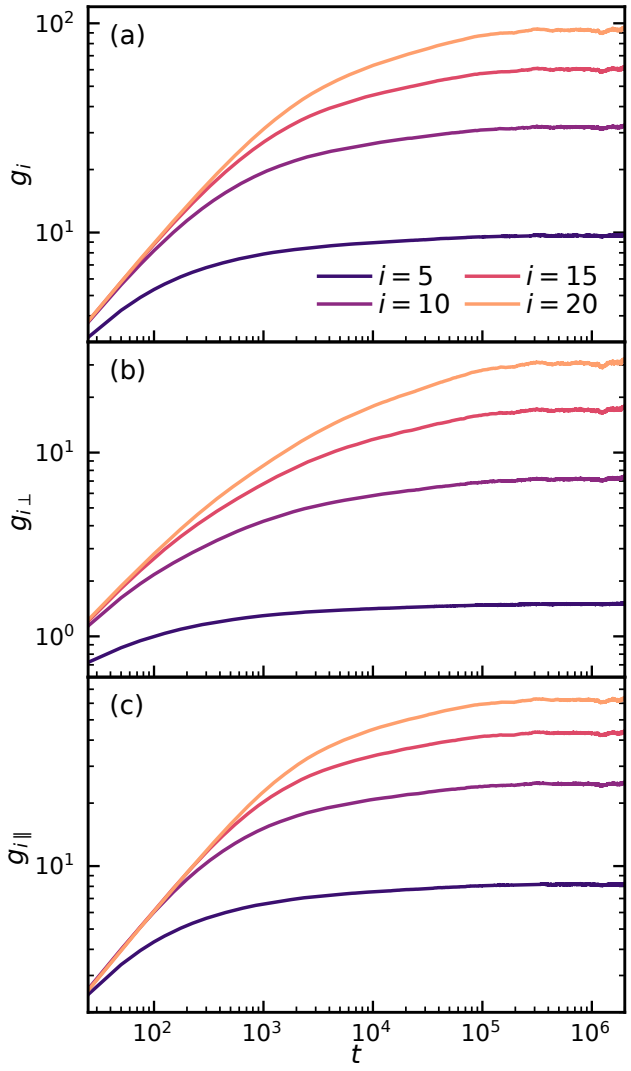

Figure S7: Mean-squared displacements of monomers with different indices i computed from LD simulations of a single polymer chain grafted to the NP. The panels show (a) the total MSD and the components (b) perpendicular and (c) parallel to the NP surface.

References

(S1) Poblete, S.; Wysocki, A.; Gompper, G.; Winkler, R. G. Hydrodynamics of discrete-particle models of spherical colloids: A multiparticle collision dynamics simulation study. *Phys. Rev. E* **2014**, *90*, 033314.

(S2) Wani, Y. M.; Kovakas, P. G.; Nikoubashman, A.; Howard, M. P. Diffusion and sedimentation in colloidal suspensions using multiparticle collision dynamics with a discrete particle model. *J. Chem. Phys.* **2022**, *156*, 024901.

(S3) Edmundson, J. R. The distribution of point charges on the surface of a sphere. *Acta Crystallogr. A* **1992**, *48*, 60–69.

(S4) Bishop, M.; Kalos, M. H.; Frisch, H. L. Molecular dynamics of polymeric systems. *J. Chem. Phys.* **1979**, *70*, 1299–1304.

(S5) Weeks, J. D.; Chandler, D.; Andersen, H. C. Role of repulsive forces in determining the equilibrium structure of simple liquids. *J. Chem. Phys.* **1971**, *54*, 5237–5247.

(S6) HOOMD-blue: A Python package for high-performance molecular dynamics and hard particle Monte Carlo simulations. *Comput. Mater. Sci* **2020**, *173*, 109363.

(S7) Howard, M. P.; Panagiotopoulos, A. Z.; Nikoubashman, A. Efficient mesoscale hydrodynamics: Multiparticle collision dynamics with massively parallel GPU acceleration. *Comput. Phys. Commun.* **2018**, *230*, 10–20.

(S8) Chen, R.; Poling-Skutvik, R.; Nikoubashman, A.; Howard, M. P.; Conrad, J. C.; Palmer, J. C. Coupling of nanoparticle dynamics to polymer center-of-mass motion in semidilute polymer solutions. *Macromolecules* **2018**, *51*, 1865–1872.

(S9) Allahyarov, E.; Gompper, G. Mesoscopic solvent simulations: Multiparticle-collision dynamics of three-dimensional flows. *Phys. Rev. E* **2002**, *66*, 36702.

(S10) Noguchi, H.; Kikuchi, N.; Gompper, G. Particle-based mesoscale hydrodynamic techniques. *EPL (Europhysics Lett.)* **2007**, *78*, 10005.

(S11) Ihle, T.; Kroll, D. M. Stochastic rotation dynamics: a Galilean-invariant mesoscopic model for fluid flow. *Phys. Rev. E* **2001**, *63*, 020201.

(S12) Huang, C.-C. C.; Winkler, R. G.; Sutmann, G.; Gompper, G. Semidilute polymer solutions at equilibrium and under shear flow. *Macromolecules* **2010**, *43*, 10107–10116.

(S13) Poling-Skutvik, R.; Olafson, K. N.; Narayanan, S.; Stingaciu, L.; Faraone, A.; Conrad, J. C.; Krishnamoorti, R. Confined Dynamics of Grafted Polymer Chains in Solutions of Linear Polymer. *Macromolecules* **2017**, *50*, 7372–7379.

(S14) Lo Verso, F.; Egorov, S. A.; Milchev, A.; Binder, K. Spherical polymer brushes under good solvent conditions: Molecular dynamics results compared to density functional theory. *J. Chem. Phy.* **2010**, *133*, 184901.